

**Evolution of the band-gap and band-edge energies of the lattice-matched Ga In As Sb/  
Ga Sb and Ga In As Sb/In As alloys as a function of composition**

Rita Magri, Alex Zunger, and H. Kroemer

Citation: *Journal of Applied Physics* **98**, 043701 (2005); doi: 10.1063/1.2010621

View online: <http://dx.doi.org/10.1063/1.2010621>

View Table of Contents: <http://scitation.aip.org/content/aip/journal/jap/98/4?ver=pdfcov>

Published by the **AIP Publishing**

---

**Articles you may be interested in**

[Biaxial strain-modified valence and conduction band offsets of zinc-blende GaN, GaP, GaAs, InN, InP, and InAs, and optical bowing of strained epitaxial InGaN alloys](#)  
*Appl. Phys. Lett.* **81**, 4377 (2002); 10.1063/1.1524299

[Band gaps of lattice-matched \(Ga,In\)\(As,N\) alloys](#)  
*Appl. Phys. Lett.* **75**, 2578 (1999); 10.1063/1.125083

[Band offsets at GaInP/AlGaInP\(001\) heterostructures lattice matched to GaAs](#)  
*Appl. Phys. Lett.* **73**, 1098 (1998); 10.1063/1.122096

[Band offsets at the InAlGaAs/InAlAs \(001\) heterostructures lattice matched to an InP substrate](#)  
*J. Appl. Phys.* **83**, 5852 (1998); 10.1063/1.367443

[Calculation of valence-band offsets of lattice-matched GaInTIP/InP heterostructures and of Schottky barrier heights of metal-GaInTIP contacts](#)  
*Appl. Phys. Lett.* **71**, 1231 (1997); 10.1063/1.119860

---

Frustrated by old technology?      Is your AFM dead and can't be repaired?      Sick of bad customer support?



**It is time to upgrade your AFM**  
Minimum \$20,000 trade-in discount  
for purchases before August 31st

**Asylum Research is today's  
technology leader in AFM**

[dropmyoldAFM@oxinst.com](mailto:dropmyoldAFM@oxinst.com)

**OXFORD  
INSTRUMENTS**  
*The Business of Science®*

# Evolution of the band-gap and band-edge energies of the lattice-matched GaInAsSb/GaSb and GaInAsSb/InAs alloys as a function of composition

Rita Magri<sup>a)</sup>

*Instituto Nazionale per la Fisica della Materia (INFN)-S<sup>3</sup> and Dipartimento di Fisica, Università di Modena e Reggio Emilia, Modena 41100, Italy*

Alex Zunger

*National Renewable Energy Laboratory, Golden, Colorado 80401*

H. Kroemer

*Department of Electrical and Computer Engineering, University of California and Santa Barbara (UCSB), Santa Barbara, California 93106*

(Received 29 November 2004; accepted 8 July 2005; published online 16 August 2005)

Using atomistic pseudopotential calculations we predict the evolution of the valence-band maximum energy  $E_v(x,y)$  and conduction-band minimum energy  $E_c(x,y)$  for a compositionally graded quaternary  $\text{Ga}_{1-y}\text{In}_y\text{As}_x\text{Sb}_{1-x}$  alloy lattice matched to GaSb or InAs as a function of  $(x,y)$  or, equivalently, as a function of distance from the substrate. We find upward-concave bowing for both  $E_c$  and  $E_v$ , in contradiction with simple interpolative models. A transition from staggered (type II) to broken-gap (type III) lineup relative to GaSb is predicted to occur at  $x=0.81$  and  $y=0.92$  on a GaSb substrate, and at  $x=0.59$  and  $y=0.62$  on an InAs substrate. In the latter case, the quaternary alloy has a minimum gap at  $x=0.85$  and  $y=0.87$ . © 2005 American Institute of Physics. [DOI: 10.1063/1.2010621]

## I. INTRODUCTION

The materials belonging to the “6.1 Å lattice-constant family” of semiconductors InAs, GaSb, and AlSb are becoming increasingly important for a large variety of applications, ranging from transistors [both bipolar and field-effect transistors (FETs)], to infrared detectors, photomixers, resonant tunnel diodes, and superlattices for quantum cascade lasers and other applications.<sup>1</sup> All these heterostructure devices involve at least two of the three semiconductors of the family. The two dominant properties in such heterointerfaces are the fact that: (i) GaAs, InAs, InSb, and GaSb have an unusual set of band alignments<sup>2,3</sup> (Fig. 1) spanning type-I “straddling” arrangement in GaAs/InAs, GaSb/InSb, and GaSb/GaAs, as well as type-III “broken-gap” arrangement in InAs/InSb and InAs/GaSb; and (ii) by simultaneously adjusting the alloy composition  $(x,y)$  in a particular fashion  $x=f(y)$ , it is possible to maintain a fixed lattice constant  $a(x,y)$  for the entire  $\text{Ga}_{1-y}\text{In}_y\text{As}_x\text{Sb}_{1-x}$  composition range. For example, one can select a function  $x=f(y)$  so that  $a(x,y) \equiv a_{\text{GaSb}}$ , thus the alloy can be grown lattice matched on a GaSb substrate. This can be accomplished by starting with GaSb, then adding both a fraction  $y$  of In and a fraction  $x$  of As in a graded fashion (e.g., 1% composition change per monolayer), reaching eventually the ternary  $\text{InAs}_{0.89}\text{Sb}_{0.11}$  which is lattice matched to GaSb. Given (i) and (ii) above, it is interesting to inquire how would the alloy band gap  $E_g(x,y)$  and the valence as well as the conduction-band edges  $E_v(x,y)$  and  $E_c(x,y)$  depend on the composition  $(x,y)$  under lattice-matched conditions. To investigate the behavior of band lineups under com-

positional grading is important: for example, high-speed bipolar transistors increasingly employ designs in which the energy gap in the base regions decreases from emitter to collector to speed up the flow of minority carriers. In fact, the technology of transistors based on Si/Ge alloys<sup>4</sup> (yielding the fastest Si-based transistors) is entirely based on this principle. But the amount of grading is limited by the severe 4% lattice mismatch between Si and Ge. In a GaSb-to-InAs graded base, strain can be avoided using the quaternary system, and much larger energy-gap gradients could be employed. In order to design such a device, however, it is essential to know how exactly the energy gap varies along the

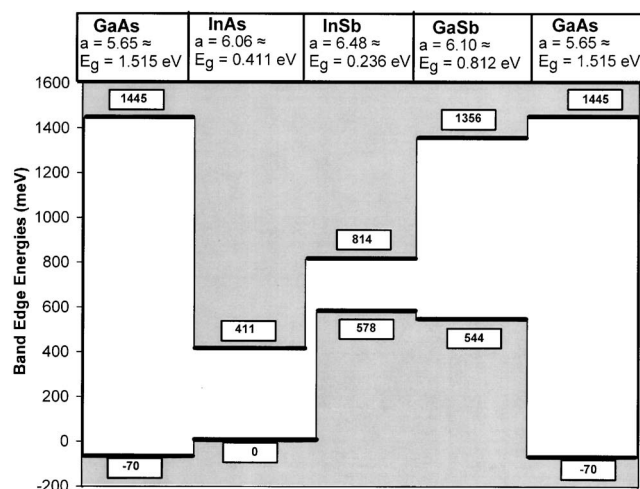


FIG. 1. Band alignment of unstrained GaAs, InAs, InSb, and GaSb binary systems. The values are obtained from empirical pseudopotential fit (see Ref. 3) to first-principles calculations (see Ref. 2) and experimental data.

<sup>a)</sup>Electronic mail: magri@unimo.it

gradient. It is also important to determine what will be the nature of the bowing (upwards or downwards) of the conduction-band minimum (CBM) and the valence-band maximum (VBM) and at which composition  $(x, y)$  would the system  $\text{Ga}_{1-y}\text{In}_y\text{As}_x\text{Sb}_{1-x}$  matched to GaSb or InAs revert from type II (staggered) to type III (broken gap). Would the band gap of the quaternary have a minimum at some intermediate  $y$ ? It is of fundamental importance to answer these questions since quaternary alloys at different compositions provide the device engineer with a larger flexibility in the tuning of device characteristics such as band gaps and band offsets between the components. Unfortunately, while most of the band-structure parameters of binary and ternary III-V systems are known,<sup>5</sup> no analogously detailed informations about the quaternary system can be found in the literature.

The paper is organized as follows. In Sec. II we use *atomistic* elasticity, to determine the lattice-matching condition  $x=f(y)$  of the quaternary alloy  $\text{Ga}_{1-y}\text{In}_y\text{As}_x\text{Sb}_{1-x}$  with the substrate, GaSb or InAs, and compare the results with the usually employed approximations based on Vegard's Law. In Sec. III we present our atomistic empirical pseudopotential method (EPM) used to solve the band structure of the narrow gap quaternary  $\text{Ga}_{1-y}\text{In}_y\text{As}_x\text{Sb}_{1-x}$  random alloy. In Sec. IV we show our results for the valence- and conduction-band edges  $E_v$  and  $E_c$  as a function of the alloy composition  $x=f(y)$  for  $\text{Ga}_{1-y}\text{In}_y\text{As}_x\text{Sb}_{1-x}$  grown both on GaSb and InAs, and compare the results with the interpolative models widely used by the device engineers' community.<sup>5</sup> In Sec. V we determine the fraction  $y$  of In [and  $x$  of As via  $x=f(y)$ ], in the quaternary alloys grown on GaSb or InAs at which the transition from a staggered to a broken-gap lineup with the substrate takes place. Finally, in Sec. VI we compare our theoretical predictions for band alignments and band gaps with the available experimental data present in the literature.

## II. FINDING VARIOUS SUBSTRATE-MATCHING $X=F(Y)$ CONDITIONS

Here we contrast Vegard-like approximations<sup>6</sup> with atomistic strain minimizing predictions.<sup>7</sup>

### A. Vegard's law

The simplest Vegard-like approximation for a quaternary is

$$a(x, y) = xy a_{\text{InAs}} + x(1-y) a_{\text{GaAs}} + (1-x)y a_{\text{InSb}} + (1-x) \times (1-y) a_{\text{GaSb}}. \quad (1)$$

The condition  $a(x, y) \equiv a_s$ , (with  $a_s = a_{\text{GaSb}}$  or with  $a_s = a_{\text{InAs}}$ ) leads to the function  $x=f_{\text{Vegard}}(y)$  for which  $\text{Ga}_{1-y}\text{In}_y\text{As}_x\text{Sb}_{1-x}$  is lattice-matched to GaSb. Other approximations include the linear  $x=0.89y$  rule obtained by considering the quaternary alloy  $\text{Ga}_{1-y}\text{In}_y\text{As}_x\text{Sb}_{1-x}$  as the solid solution<sup>5</sup> of GaSb and the lattice-matched ternary  $\text{InAs}_{0.89}\text{Sb}_{0.11}$  alloy, that is  $(\text{GaSb})_z(\text{InAs}_{0.89}\text{Sb}_{0.11})_{1-z}$ , and the expression  $x=0.866y/(1-0.048y)$ , also proposed in literature.<sup>8</sup> In Fig. 2 we denote via empty symbols the result  $x=f_{\text{Vegard}}(y)$  corresponding to these approximations. We see that they have a linear trend and are very similar. We choose one of these functions as the "Vegard-like"  $x=f_{\text{Vegard}}(y)$ .

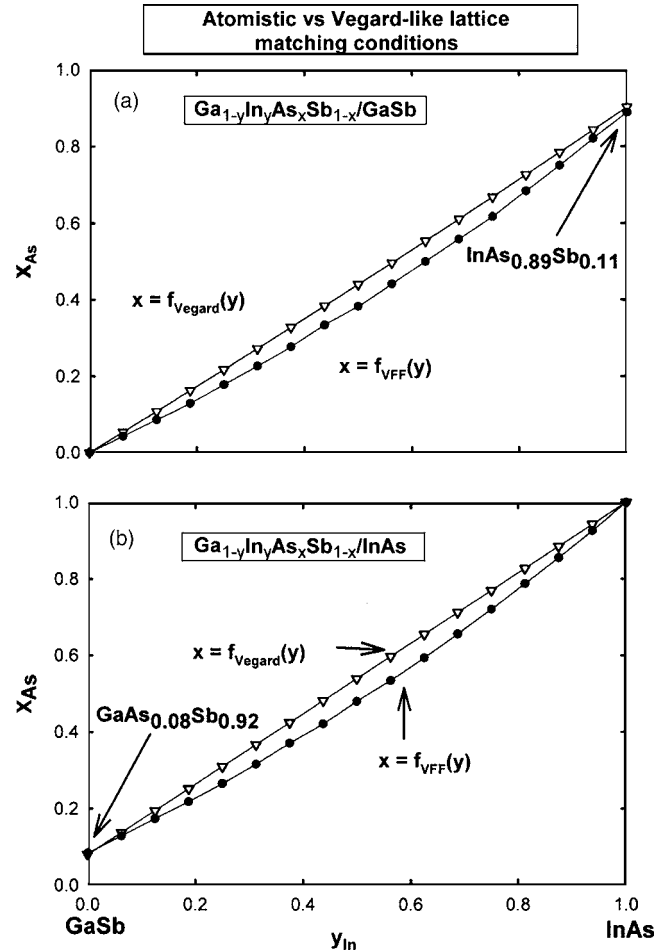


FIG. 2. As composition  $x$  as a function of In composition  $y$  giving lattice matching to the GaSb substrate (a) and to the InAs substrate (b). The relations  $x=f_{\text{Vegard}}(y)$  (empty symbols) were derived using Vegard-like relations (linear interpolations of the binary values) while the relation  $x=f_{\text{VFF}}(y)$  (full circles) was derived through the atomistic VFF calculations.

### B. Atomistic description of atomic configurations and atomistic elasticity

Vegard-like approximations derive the alloy lattice parameter  $a(x, y)$  on the basis of the alloy composition  $(x, y)$  only. However, unlike ternary alloys, (e.g.,  $A_xB_{1-x}C$ ) for which the microscopic composition  $x$  uniquely defines the number of nearest-neighbor bonds  $n_{A-C}$  and  $n_{B-C}$  of each type, for quaternary alloys, such as  $\text{Ga}_{1-y}\text{In}_y\text{As}_x\text{Sb}_{1-x}$ , a further parameter is needed to specify the nearest-neighbor bond number  $n_{i-j}$  between atoms of kind  $i$  and  $j$ . We define this "short-range order" (SRO) parameter  $\xi$  as

$$\xi = \frac{n_{\text{Ga-Sb}}}{N} - (1-y)(1-x), \quad (2)$$

where  $N$  is the total number of nearest-neighbor bonds,  $n_{\text{Ga-Sb}}$  is the actual number of Ga-Sb bonds in a particular alloy configuration, and  $(1-y)(1-x)$  is the fraction of Ga-Sb bonds in a perfectly random arrangement. Thus, for a perfect random alloy  $\xi=0$ , whereas  $\xi>0$  means that the alloy is enriched of Ga-Sb and In-As bonds and, correspondingly depleted of In-Sb and Ga-As bonds. We can say in this case that GaInAsSb can be described as an alloy constituted mainly by InAs+GaSb. On the other hand,  $\xi<0$  means that

InSb+GaAs is the correct description since In–Sb plus Ga–As bonds are the majority.

To decide what atomic arrangement is thermodynamically the more appropriate one for  $\text{Ga}_{1-y}\text{In}_y\text{As}_x\text{Sb}_{1-x}$ , one can proceed as in Ref. 9 and minimize the energy functional,

$$E_{\text{tot}}(\{S_i\}, \{\mathbf{R}_i, i=1, \dots, N\}) = E_{\text{chem}}(\{S_i\}, \{\mathbf{R}_i, i=1, \dots, N\}) + E_{\text{strain}}(\{S_i\}, \{\mathbf{R}_i, i=1, \dots, N\}), \quad (3)$$

where  $\{S_i\}$  indicates that  $E_{\text{tot}}$ ,  $E_{\text{chem}}$ , and  $E_{\text{strain}}$  are functionals of the atomic configurations  $S_i$  obtained by differently arranging the cations (Ga, In) and the anions (As, Sb) on the  $N$  sites of a zinc-blende lattice. In Eq. (3)

$$E_{\text{chem}} = \frac{1}{2} \sum_i \sum_{j=1}^{nm} E_{ij} n_{i-j}, \quad (4)$$

where  $n_{i-j}$  is the number of bonds of type  $i-j$ , and  $E_{ij}$  is the respective bond energy for which we use the experimental cohesive energy per bond given in Ref. 10 for binary compound  $ij$ . For GaInAsSb we use 1.63, 1.55, 1.48, and 1.40 eV for GaAs, InAs, GaSb, and InSb, respectively. It turns out that using these values for the bond cohesive energies,  $E_{\text{chem}}$  has a negligible contribution to the energy functional  $E_{\text{tot}}$ , thus the thermodynamic stability is decided by  $E_{\text{strain}}$ . In fact, the chemical energy difference between two configurations is given by  $\Delta E_{\text{chem}} = \Delta n[(E_{\text{GaSb}} + E_{\text{InAs}}) - (E_{\text{GaAs}} + E_{\text{InSb}})]$ , since a change  $\Delta n$  of the number of Ga–Sb (and In–As) bonds corresponds to a change  $-\Delta n$  of In–Sb (and Ga–As) bonds if composition  $(x, y)$  has to remain unchanged. With the values reported above for  $E_{ij}$  it is easy to show that  $\Delta E_{\text{chem}} = 0$ .

For the strain energy we use the valence force field (VFF) approach<sup>11,12</sup> where the total strain energy of the system is written as a sum of bond-stretching ( $\alpha$ ) and bond-bending ( $\beta$ ) forces

$$E_{\text{strain}} = \sum_i \frac{3}{8d_{0i}^2} \alpha_i (\mathbf{r}_i \cdot \mathbf{r}_i - d_{0i}^2)^2 + \sum_{i,j} \frac{3}{8d_{0i}^2 d_{0j}^2} \beta_{i,j} \left( \mathbf{r}_i \cdot \mathbf{r}_j + \frac{1}{3} d_{0i}^2 d_{0j}^2 \right)^2, \quad (5)$$

where the first sum runs over all the distinct nearest-neighbor bonds  $i$  while the second sum is over all the bonding angles formed by bonds  $i$  and  $j$ . These two terms represent the strain energy due to bond-length stretching and bond angle distortions. We use the bond-stretching  $\alpha_i$  and the bond bending  $\beta_{i,j}$  force constants of Ref. 12

Using the four bond lengths  $d_{0i} = 2.448, 2.622, 2.640,$  and  $2.805 \text{ \AA}$  for the Ga–As, In–As, Ga–Sb, and In–Sb bonds, respectively, we see that creating InAs+GaSb bonds exerts less strain than creating InSb+GaAs bonds.

A minimization of the energy functional of Eq. (3) versus configuration  $S_i$  generally gives atomic configurations with nonzero  $\xi$  parameters. Such a minimization is done by occupying the cation sublattice by Ga or In, and the anion sublattice by As or Sb, and scanning via Monte Carlo many such occupation patterns at a given  $T$  until  $E_{\text{tot}}$  of Eq. (3) is

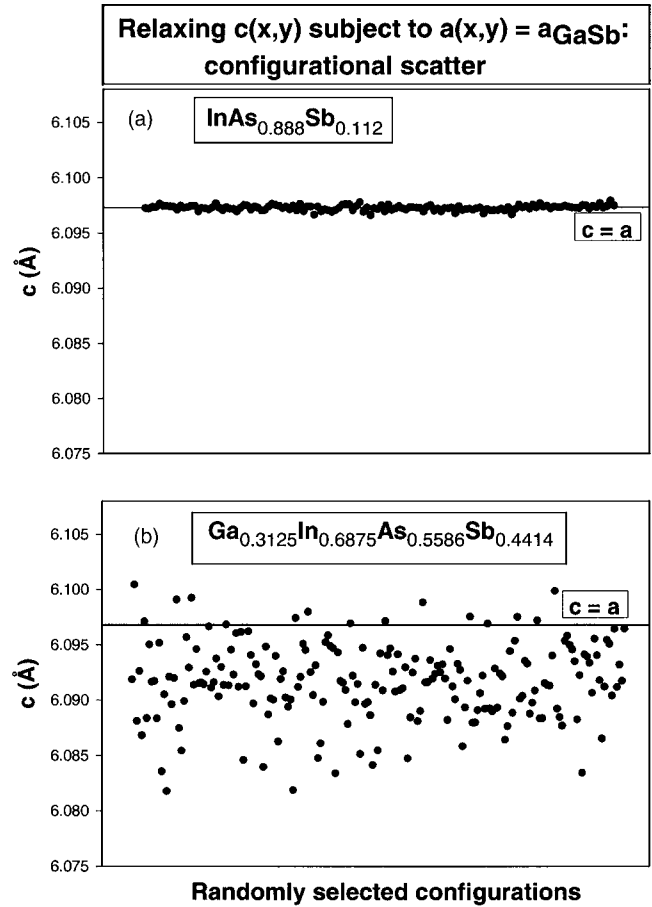


FIG. 3.  $c$ -axis values obtained using around 200 different atomic configurations of the ternary  $\text{InAs}_{0.888}\text{Sb}_{0.112}$  (a) and of the quaternary  $\text{Ga}_{0.3125}\text{In}_{0.6875}\text{As}_{0.5586}\text{Sb}_{0.4414}$  (b) alloys.

minimum. This will be discussed briefly in Sec. VI, in which we find  $\xi > 0$  for InGaAsSb at moderate temperatures. However, it is instructive to treat the  $\xi = 0$  case as well. Thus, in Secs. IV, V, and VI A we assume a random occupation of the sites, then relax the atomic positions, and then solve the Schrödinger equation, finding band energies and band gaps.

We have modeled the random  $\text{Ga}_{1-y}\text{In}_y\text{As}_x\text{Sb}_{1-x}$  alloy by a large supercell ( $4 \times 4 \times 4$ , in units of the lattice parameter  $a$ ) occupying its 512 lattice sites randomly by the atoms Ga, In, As, and Sb according to specified compositions  $(x, y)$ . For each generated configuration  $S_i$  we have minimized the total elastic energy of Eq. (2) by keeping the in-plane lattice parameter  $a(x, y) = a_s$  fixed and obtaining the atomic equilibrium positions and the equilibrium  $c$  lattice parameter of the cell. We found a configurational fluctuation (within  $0.02 \text{ \AA}$ ) of the lattice parameters  $c(x, y)$  for each composition  $(x, y)$ . We illustrate this fluctuation in Fig. 3 where we show the  $c(x, y)$  values calculated for the fixed in-plane lattice parameter  $a_s = a_{\text{GaSb}}$  for different atomic configurations of the ternary  $\text{InAs}_{0.888}\text{As}_{0.112}$  alloy [Fig. 3(a)] and of the quaternary  $\text{Ga}_{0.3125}\text{In}_{0.6875}\text{As}_{0.5586}\text{Sb}_{0.4414}$  alloy [Fig. 3(b)]. We see a small scatter in the  $c$  axis of the ternary alloy and a larger one in the case of the quaternary alloy. This is due to the fact that the quaternary alloy has four distinct bonds: Ga–As, Ga–Sb, In–As, and In–Sb and eight different bond angles that can be formed by each couple of bonds. All these need

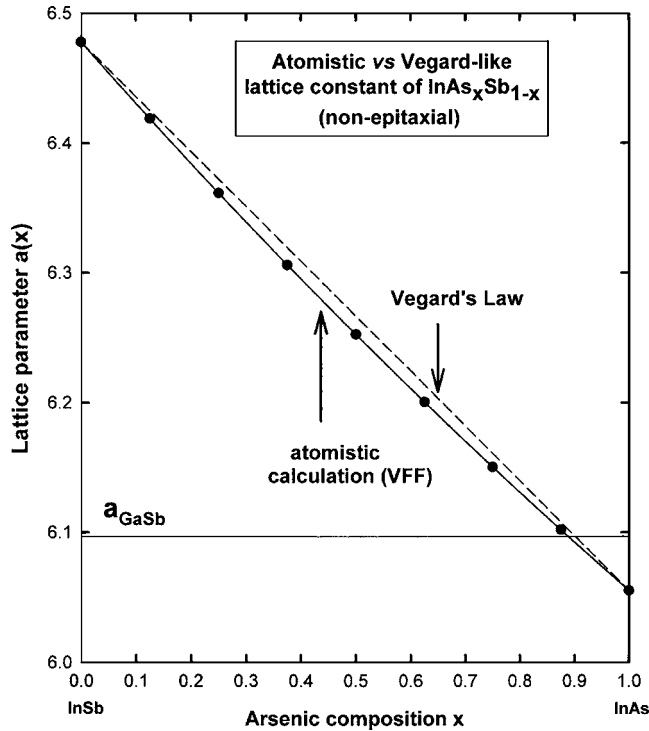


FIG. 4. Comparison of the predicted equilibrium lattice parameters  $a(x)$  of the random ternary  $\text{InAs}_x\text{Sb}_{1-x}$  alloys as a function of composition  $x$ . The predictions of Vegard's law are given by the dashed line whereas the predictions of the atomistic VFF (after averaging over 200 atomic configurations) are given by the full circles.

to be adjusted in order to minimize the elastic energy. This leads to a strong dependence of the calculated bond lengths, bond angles, and  $c$  axis at the minimum elastic energy on the initial distribution of atoms within the 512 unit cell. In the case of the ternary alloy one has to adjust only two kind of bonds In–As and In–Sb and the three different kind of bond angles, thus the final minimum energy configuration is less sensitive to the initial choice of the atomic positions.

To each fixed In fraction  $y$ , there corresponds a small range  $\Delta x$  of possible As compositions  $x$  for which the quaternary alloy is lattice matched to its substrate. By averaging over a number of different atomic configurations we calculate the quaternary alloy lattice parameter  $a(x, y)$  which satisfies the matching condition with the substrate. The lattice parameter  $a(x, y)$  obtained using the atomistic calculations turns out to be different from the Vegard-like behavior given by Eq. (1). This is true even in the simpler case of ternary alloys, as seen in Fig. 4 which compares the lattice constant  $a(x)$  of the ternary  $\text{InAs}_x\text{Sb}_{1-x}$  alloy given by Vegard's law (dashed line) with that obtained by the atomistic calculation (averaged over a large number of different atomic configurations, full dots). The lattice parameter predicted by the atomistic elasticity departs from the linear Vegard trend mostly around composition  $x=0.5$ , where the In–As and In–Sb bonds are both more numerous and maximally strained. This departure of the atomistically predicted lattice parameters from a composition weighted Vegard average is present also in the quaternary alloys. This leads to different functions  $x = f_{\text{VFF}}(y)$  (shown in Fig. 2) for the compositions at which the quaternary alloy is lattice matched to the GaSb and InAs substrates. A fit yields

$$x = 0.001 + 0.648y + 0.239y^2 \quad (6)$$

on GaSb substrate [ $x = f_{\text{VFF}}(y)$  in Fig. 2(a)] and

$$x = 0.086 + 0.656y + 0.256y^2 \quad (7)$$

on InAs substrate [ $x = f_{\text{VFF}}(y)$  in Fig. 2(b)]. These functions show a larger bowing term than the Vegard-like functions  $x = f(y)$ .

### III. METHOD OF CALCULATION OF THE ELECTRONIC STRUCTURE

We use an atomistic empirical pseudopotential method to calculate the band structure. Once the atomic positions are relaxed so as to minimize the total strain energy (Sec. II), we next assign to each relaxed atom a pseudopotential  $v_\alpha$  and construct the total potential of the supercell by superposing individual pseudopotentials  $V(\mathbf{r}) = \sum_{\alpha, n} v_\alpha(\mathbf{r} - \mathbf{r}_\alpha - \mathbf{R}_n)$  yielding the “single-particle” Hamiltonian,

$$\left[ -\frac{\beta}{2} \nabla^2 + \sum_{n\alpha} v_\alpha(\mathbf{r} - \mathbf{R}_{n\alpha}) \right] \psi_i(\mathbf{r}) = \epsilon_i \psi_i(\mathbf{r}), \quad (8)$$

where  $\mathbf{R}_{n\alpha}$  denotes the position of the  $n$ th ion of type  $\alpha$  (=In, Ga, As, and Sb). This gives the wave functions  $\psi_i(\mathbf{r})$  and the eigenvalues  $\epsilon_i$ . The term  $\beta$ , which scales the kinetic energy in the Schrödinger equation, has been introduced to represent the quasiparticle nonlocal self-energy effects:<sup>13</sup> it allows one to simultaneously fit bulk effective masses and band gaps. Using the 512 atom unit cell we create many atomistic realizations of the quaternary  $\text{Ga}_{1-y}\text{In}_y\text{As}_x\text{Sb}_{1-x}$  alloy at different compositions  $(x, y)$  satisfying the lattice-matching conditions  $x = f_{\text{Vegard}}(y)$  and  $x = f_{\text{VFF}}(y)$ . The Hamiltonian diagonalization gives us the electronic structure as a function of the lattice-matching conditions from which we derive the evolution of the conduction-band  $E_c(x, y)$  and valence-band  $E_v(x, y)$  edges as a function of  $(x, y)$ , or equivalently of the distance  $Z$  from the substrate, when the alloy composition is graded along the growth direction.

The pseudopotential  $v_\alpha$  includes the spin-orbit interaction, thus the wave functions  $\psi_i(\mathbf{r})$  are spinors with spin-up and spin-down components. The wave functions are expanded in a plane-wave basis with a cutoff determined by fitting  $v_\alpha(\mathbf{G})$  with  $\mathbf{G}$  the reciprocal lattice vectors.  $v_\alpha(\mathbf{G})$  is fitted to the experimentally measured electron and hole effective masses,<sup>14</sup>  $\Gamma$ ,  $X$ , and  $L$  band gaps (target values at 0 K),<sup>14</sup> spin-orbit splittings,<sup>14</sup> hydrostatic deformation potentials of the band gaps,<sup>14</sup> local-density approximation (LDA)-calculated band offsets,<sup>14,15</sup> and LDA-predicted single-band-edge deformation potentials<sup>16</sup> of the four binary systems. We use the atomic pseudopotentials described in Ref. 3. The InSb potential is slightly adjusted with respect to that of Ref. 3 so that the VBM position of InSb agrees better with the recent experimental data.<sup>5</sup> In Fig. 1 we report the band alignments between the unstrained binary systems. The technical details of our method and examples of its successful application to the description of abrupt and segregated superlattices and free standing ternary alloys are given elsewhere.<sup>3</sup>

Our method has two main advantages over the density-functional theory (DFT)-LDA self-consistent calculations:

first, it does not have the “band-gap error” problem,<sup>17</sup> thus the band gaps are in good agreement with the experimental values. *Second*, because of the small cutoff needed in  $v_\alpha(\mathbf{G})$  the method is much faster computationally, and thus can treat systems with hundreds and thousands of atoms per unit cell. This is essential for the description of random alloys where the configurational and atomic disorder effects are relevant. Such effects are often neglected by the virtual crystal approximation (VCA) currently employed together with self-consistent DFT-LDA calculations.<sup>18</sup>

Our scheme has also the following advantages over the method of Ref. 19. First, differently from Ref. 19, we describe all the four bonds present in GaInAsSb on the same footing, thus, not only In–As and Ga–Sb bonds, but also Ga–As and In–Sb bonds are taken into account. This allows us to treat in exactly the same way and with the same accuracy both superlattices (SLs) and alloy systems. In the case of superlattices, where Ga–As and In–Sb bonds are necessarily present at the interfaces, we obtain automatically the correct  $C_{2v}$  symmetry,<sup>20</sup> the correct in-plane polarization ratio,<sup>21</sup> and the Rashba term.<sup>22</sup> Dente and Tilton,<sup>19</sup> instead, treat the potential at interfaces through a simple rectangle function, neglecting the interface-related inversion asymmetry in InAs/GaSb SLs. *Second*, we can easily take into account the effects of interfacial disorder and segregation, without the need to introduce additional fitting parameters. Indeed, we were able to account for the band-gap increase with sample growth temperature observed in InAs/GaInSb SLs.<sup>23,24</sup>

The ability to describe accurately the interfacial properties in our approach is also the main advantage over the  $\mathbf{k}\cdot\mathbf{p}$  method.<sup>25</sup> To obtain the correct  $C_{2v}$  symmetry and, thus describe the experimental observations related to the interfacial inversion asymmetry in InAs/GaSb,  $\mathbf{k}\cdot\mathbf{p}$  schemes must add to the Hamiltonian a term (or boundary condition) with one or two free parameters, whose values are determined heuristically by fitting the experiment and, thus are defined *a posteriori*.<sup>26,27</sup> This procedure obviously cannot be used to provide predictions, only fits to known experiments. In our scheme, instead, the system symmetry is decided automatically by the atomic positions and is therefore an output of the calculation, allowing us to predict the electronic properties.

#### IV. BOWING OF BAND-EDGE ENERGIES

Figure 5(a) shows the pseudopotential calculated conduction-band edge  $E_c$  and valence-band edge  $E_v$  profiles calculated for the GaSb substrate and  $x=f_{\text{VFF}}(y)$  as a function of the In concentration  $y$  (top axis) and of the distance  $Z$  from the GaSb substrate (bottom axis) when the alloy composition  $y$  is graded along the growth direction at a rate of 1% per monolayer. For comparison we show as dashed lines the simplified conduction- and valence-band edge positions proposed in Ref. 8. If we use the lattice-matching condition  $x=f_{\text{Vegard}}(y)$  instead of  $x=f_{\text{VFF}}(y)$  we obtain in the pseudopotential calculation for  $E_v$  and  $E_c$  very similar trends as shown in Fig. 6: the  $E_v$  and  $E_c$  values obtained using Vegard’s law are always lower than those obtained using VFF by a maximum difference of only 40–50 meV.

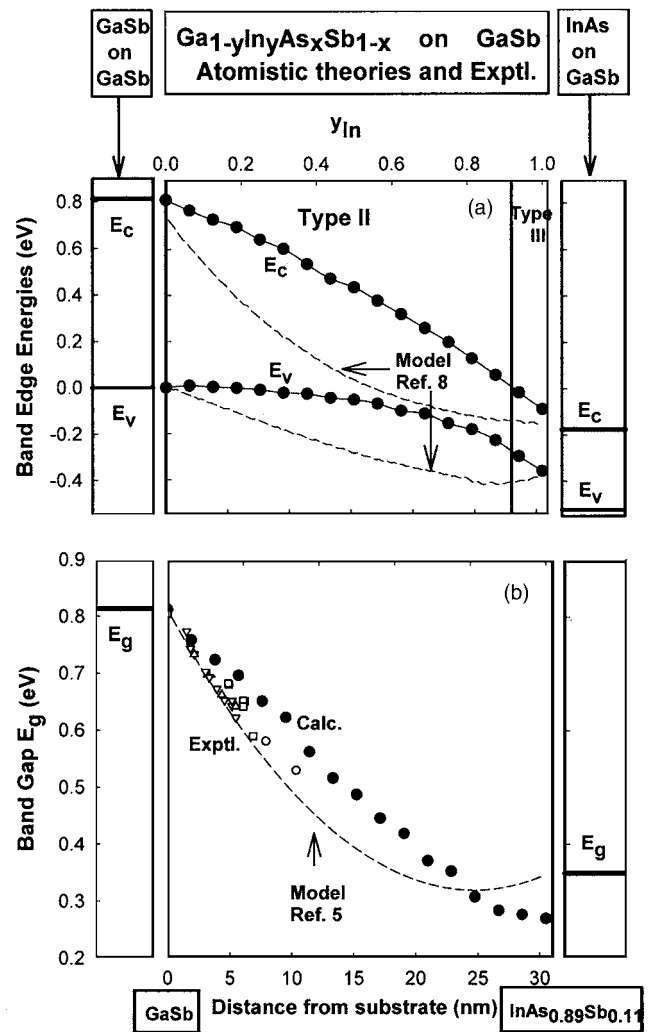


FIG. 5. (a) Conduction- and valence-band edge profiles of the quaternary random Ga<sub>1-y</sub>In<sub>y</sub>As<sub>x</sub>Sb<sub>1-x</sub> alloy grown on GaSb as a function of In concentration  $y$ . The dashed curves are the band-edge positions proposed in Ref. 8 for  $T=300$  K. (b) Band gap of Ga<sub>1-y</sub>In<sub>y</sub>As<sub>x</sub>Sb<sub>1-x</sub>/GaSb as a function of In concentration  $y$  (top axis) and distance from the GaSb substrate (bottom axis). The calculated values can be fit with the cubic polynomial  $E_g(y) = 0.804 - 0.5257y - 0.4322y^2 + 0.4175y^3$ . Experimental data translated to  $T=0$  K (see text) were obtained by PL measurements [(Ref. 31) empty circles, (Ref. 30) empty downward triangles, and (Ref. 28) crosses], electroreflectance [(Ref. 29) empty squares], and IR absorption [(Ref. 32) empty upward triangles]. The dashed line is the relation proposed for  $E_g$  at  $T=0$  K in Ref. 5. The horizontal lines at the far left and far right sides represent the band edges and band gaps of the GaSb and InAs binary compounds grown on GaSb, as indicated.

What is striking in Figs. 5 and 6 is that the atomistic calculations predict a small but *negative* (upwards concave) bowing of  $E_c$  and a pronounced upward bowing of  $E_v$ . This is in contrast with the behavior usually proposed in literature<sup>8</sup> (dashed lines in Fig. 5) and based on calculations using interpolative schemes, where the bowing of  $E_c$  is predicted to be *positive* (downwards concave) and much larger than the bowing of  $E_v$ . The predictions for the conduction- and valence-band edges of the quaternary alloy grown on an InAs substrate are shown in Fig. 7(a). We find similar trends of the band edges with composition as in the case of the quaternary grown on GaSb: a pronounced upward bowing of  $E_v$  and a slight upward bowing of  $E_c$ . Depending on the

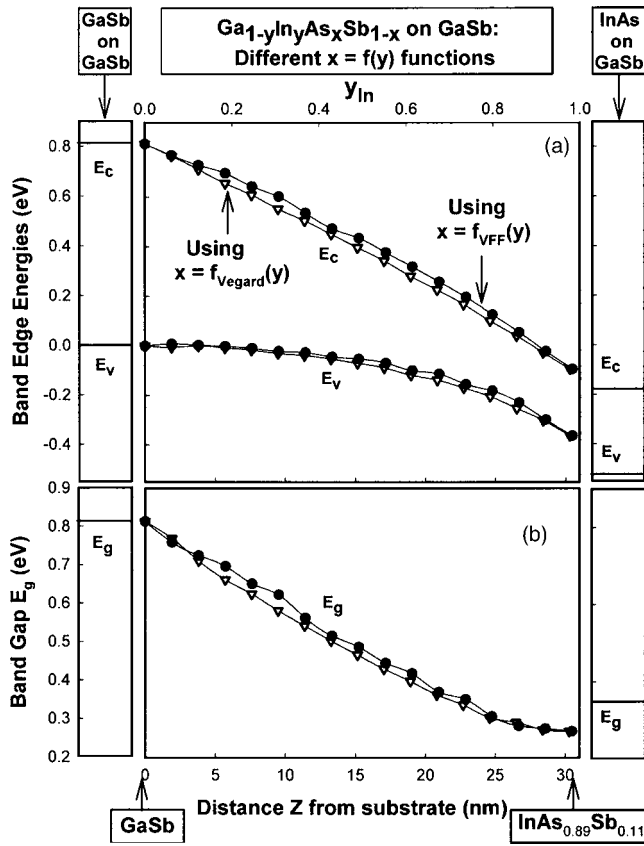


FIG. 6. Comparison of: (a) the valence- and conduction-band edges and (b) band gaps of the quaternary  $\text{Ga}_{1-y}\text{In}_y\text{As}_x\text{Sb}_{1-x}/\text{GaSb}$  alloy calculated using the Vegard-like lattice-matching functions  $x=f_{\text{Vegard}}(y)$  (downward empty triangles) with the  $x=f_{\text{VFF}}(y)$  extracted by the atomistic VFF calculations (full circles).

device application, the free passage of electrons from the InAs conduction band to the GaSb valence band could be either desirable (Ohmic contacts between  $n$  and  $p$ ) or it could be a nuisance. The strong positive bowing of the valence-band edge found in this work (see Figs. 5–7) shows that grading should be avoided at all cost if interband transport is desirable, but would be very beneficial to the opposite objective.

To understand the unexpected negative bowings of the conduction-band edges in Figs. 5 and 7 we first note that they are displayed with respect to the standard<sup>5</sup> linear interpolation of band edges of GaSb and  $\text{InAs}_{0.89}\text{Sb}_{0.11}$  (for the GaSb substrate, Fig. 5), and InAs and  $\text{GaAs}_{0.08}\text{Sb}_{0.92}$  (for the InAs substrate, Fig. 7). These reference materials have almost exclusively Ga–Sb and In–As bonds with a very small percentage of In–Sb bonds (for the GaSb substrate) or Ga–As bonds (for the InAs substrate). This choice of end-point reference materials is different from the usual practice in ternary alloys, such as  $\text{InAs}_x\text{Sb}_{1-x}$  where the bowing is valued relatively to the linear interpolation  $x(\text{InAs})+(1-x)(\text{InSb})$  of the two end-point materials InAs and InSb. The latter is a consistent choice since the ternary alloy has the same bonds (In–As and In–Sb) as the end points. But in the quaternary alloy  $\text{Ga}_{1-y}\text{In}_y\text{As}_x\text{Sb}_{1-x}$  four bonds Ga–Sb, In–As, In–Sb, and Ga–As are present, yet they are not considered when the quaternary is considered as the superposition of

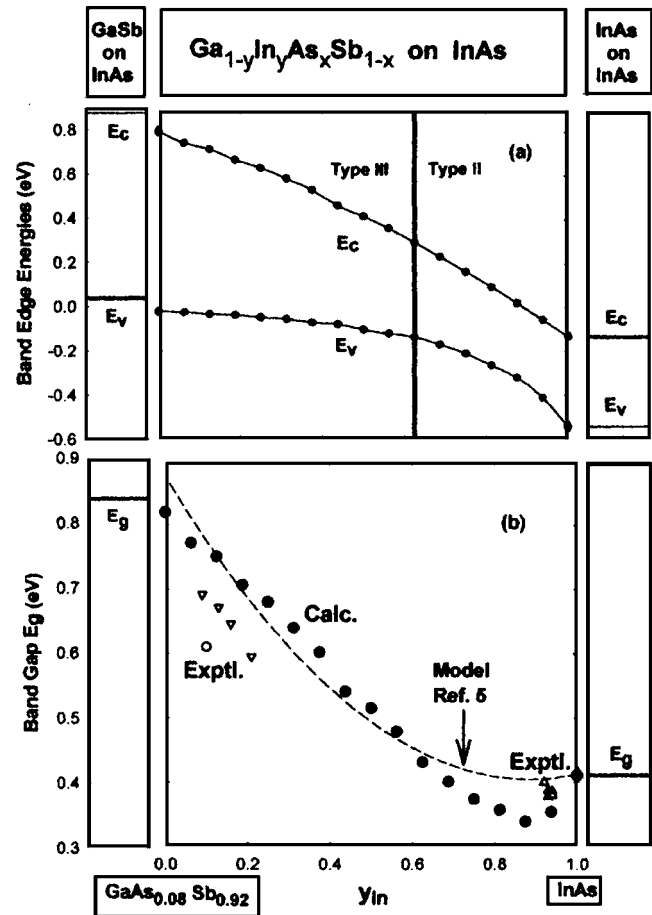


FIG. 7. (a) Conduction- and valence-band edge profiles of the quaternary  $\text{Ga}_{1-y}\text{In}_y\text{As}_x\text{Sb}_{1-x}$  alloy grown on InAs as a function of In concentration  $y$ . (b) Band gaps of  $\text{Ga}_{1-y}\text{In}_y\text{As}_x\text{Sb}_{1-x}/\text{InAs}$  as a function of In concentration  $y$ . The horizontal lines at the far left and right sides have the same meaning as in Fig. 5. The dashed line is the band gap vs  $y$  behavior proposed in Ref. 5. Downward triangles: PL measurements from Ref. 36; upward triangles: PL measurements from Ref. 38; and empty circle: PL measurement from Ref. 33.

(GaSb) and ( $\text{InAs}_{0.89}\text{Sb}_{0.11}$ ) (for the GaSb substrate) or as the superposition of (InAs) and ( $\text{GaAs}_{0.08}\text{Sb}_{0.92}$ ) (for the InAs substrate).

To illustrate how bowing depends on reference energies, we show in Fig. 8 for the quaternary alloy grown on InAs by the solid circles the energy  $\Delta E_c[x=f(y);y]$  of the EPM-calculated conduction-band minimum  $E_c$  with respect to the conventional reference energy  $E^{\text{TR}}(y)$  of ternary end points,

$$\Delta E_c^{\text{TR}}[x=f(y);y] = E_c(\text{Ga}_{1-y}\text{In}_y\text{As}_x\text{Sb}_{1-x}/\text{InAs}) - E^{\text{TR}}(y), \quad (9)$$

where

$$E^{\text{TR}}(y) = yE_c(\text{InAs}) + (1-y)E_c(\text{GaAs}_{0.08}\text{Sb}_{0.92}/\text{InAs}). \quad (10)$$

We see that  $\Delta E_c^{\text{TR}} > 0$ , implying negative bowing  $b < 0$  [as also seen by the solid circles in Fig. 7(a)]. To see that this  $b < 0$  is merely an artifact of selecting  $E^{\text{TR}}(y)$  of Eq. (10) as a reference, we also show in Fig. 8 the energy of the conduction-band minimum (solid circles) with respect to the alternative reference energy  $E^{\text{BR}}(y)$  of binary constituents,

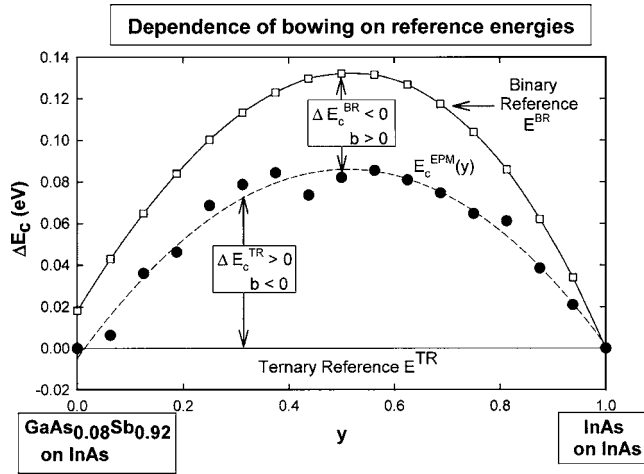


FIG. 8. Difference of the conduction-band energy  $\Delta E_c$  of the EPM calculated  $E_c(\text{Ga}_{1-y}\text{In}_y\text{As}_x\text{Sb}_{1-x}/\text{InAs})$  with respect to the linear interpolation  $yE_c(\text{InAs}) + (1-y)E_c(\text{GaAs}_{0.08}\text{Sb}_{0.92})$  ( $E^{\text{TR}}$ ) (full circles). The difference  $\Delta E_c$  of  $E^{\text{BR}}$  [Eq. (11)] and  $E^{\text{TR}}$  is shown by empty squares. The dashed line is a parabolic fit of the EPM calculated values (full circles).

$$E^{\text{BR}}(y) = xyE_c^{\text{InAs}} + x(1-y)E_c^{\text{GaAs}} + (1-x)yE_c^{\text{InSb}} + (1-x) \times (1-y)E_c^{\text{GaSb}}. \quad (11)$$

Given

$$\Delta E_c^{\text{BR}}[x=f(y);y] = E_c(\text{Ga}_{1-y}\text{In}_y\text{As}_x\text{Sb}_{1-x}/\text{InAs}) - E^{\text{BR}}(y), \quad (12)$$

we see that  $\Delta E_c^{\text{BR}} < 0$ , implying a bowing  $b > 0$ , as normally expected. Since the reference  $E^{\text{BR}}(y) > E^{\text{TR}}(y)$  we see that the effect of the In–Sb and Ga–As bonds [included in  $E^{\text{BR}}(y)$  [Eq. (11)], but almost missing in  $E^{\text{TR}}(y)$  [Eq. (10)] is to increase the energy of the conduction-band edge. Our atomistic model for the quaternary random alloys (see Sec. II) correctly includes all four In–As, Ga–Sb, Ga–As, and In–Sb bonds. This explains the negative bowing of the calculated  $E_c(\text{Ga}_{1-y}\text{In}_y\text{As}_x\text{Sb}_{1-x}/\text{InAs})$  with respect to  $E^{\text{TR}}(y)$  shown in Fig. 7(a).

Our results show that the commonly employed assumption of a strong positive bowing of  $E_c$  of the quaternary alloy at composition  $x=f(y)$ ,  $y$  with respect to  $E^{\text{TR}}(y)$  is unsound in that it would imply a quaternary alloy with no In–Sb and Ga–As bonds.

## V. TRANSITION FROM TYPE-II (STAGGERED) TO TYPE-III (BROKEN GAP) ALIGNMENT

There is much interest in graded structures that span the entire alloy range and where the CBM on the In-rich side dips below the VBM on the Ga-rich side.<sup>34</sup> It is desirable to have this transition to a type III, broken gap, for materials that are as In-rich as possible, so as to have a sufficiently high electron mobility.

From Fig. 5 we can derive the following three possibilities for a broken-gap lineup:

- The CBM of a quaternary  $\text{Ga}_{1-y}\text{In}_y\text{As}_x\text{Sb}_{1-x}/\text{GaSb}$  dips below the VBM of GaSb. Because of the small and positive bowing of  $E_c(x,y)$  of the quaternary, this transition occurs for a relatively high In content of  $y_c$

$= 0.92$ . If  $E_c(x,y)$  had no bowing one would have  $y_c = 0.90$ ; using the positive bowing summarized by Ref. 8 one would predict  $y_c \approx 0.55$  with a much smaller In content.

- The CBM of  $\text{InAs}_{0.89}\text{Sb}_{0.11}$  [ $y=1$  in Fig. 5(a)] dips below the VBM of the quaternary  $\text{Ga}_{1-y}\text{In}_y\text{As}_x\text{Sb}_{1-x}$  alloy already for  $y \leq 0.6$ .
- The CBM of InAs [matched to GaSb; see the horizontal lines at far right end of Fig. 5(a)] dips below the VBM of the quaternary  $\text{Ga}_{1-y}\text{In}_y\text{As}_x\text{Sb}_{1-x}/\text{GaSb}$  alloy for  $y \leq 0.78$ . From Fig. 7(a) we can see that:
- In the case of  $\text{Ga}_{1-y}\text{In}_y\text{As}_x\text{Sb}_{1-x}/\text{InAs}$  the CBM of InAs dips below the VBM of the quaternary at  $y \leq 0.62$ . Very interestingly, the quaternary alloy reaches a well-defined minimum gap at  $y=0.87$ . The gap is 72 meV smaller than the InAs gap.

Our calculated  $E_v$  and  $E_c$  for  $\text{Ga}_{1-y}\text{In}_y\text{As}_x\text{Sb}_{1-x}/\text{GaSb}$ , Fig. 5(a), are in reasonable agreement with the experimental data of Ref. 28 where the reported conduction band offsets between  $\text{Ga}_{1-y}\text{In}_y\text{As}_x\text{Sb}_{1-x}$  and GaSb are 160, 205, and 250 meV at alloy compositions  $y=0.11$ , 0.14, and 0.18, respectively, and the valence-band offset is 50 meV at  $y=0.18$ . The corresponding values we obtain for the conduction-band (118 meV) and valence-band (15 meV) offsets at  $y=0.1825$  are somewhat smaller than the measured values. The transition from the staggered to the broken-gap alignment at about  $y=0.92$  and  $x=0.81$  is in good agreement with the recent experiments<sup>35</sup> which found a type-II staggered lineup for  $y=0.85$  and a broken-gap lineup for  $y=0.95$ . For  $y=0.92$ , they observed both types of heterojunctions depending on temperature. Our calculations, and, in particular, the strong bowing of the valence-band edge, would predict a broken-gap lineup between the quaternary alloy and the ternary GaAsSb alloy all the way up to about a  $y=0.6$  In content, much higher than expected. For the valence-band edges  $E_v$  and  $E_c$  of  $\text{Ga}_{1-y}\text{In}_y\text{As}_x\text{Sb}_{1-x}/\text{InAs}$  there is still a lack of experimental data in literature. Moiseev *et al.*<sup>36</sup> affirm that the  $\text{Ga}_{1-y}\text{In}_y\text{As}_x\text{Sb}_{1-x}/\text{InAs}$  heterostructure for  $y < 0.22$  has a broken-gap type of alignment which is in agreement with the results of the present calculation.

## VI. BAND GAPS: COMPARISON WITH EXPERIMENT

### A. Neglecting short-range order: $\xi \approx 0$

We compare here our results for the hypothetical random alloy, i.e., GaInAsSb alloys in the limit of very high growth temperatures. Such alloys are characterized by a parameter  $\xi \approx 0$  [see Eq. (2)]. To compare our calculated values for  $\text{Ga}_{1-y}\text{In}_y\text{As}_x\text{Sb}_{1-x}/\text{GaSb}$  band gaps with the experiment, we report in Fig. 5(b) the available experimental results together with the theoretical predictions for samples of composition  $y < 0.25$ . The experimental data were obtained with different experimental techniques at different sample temperatures ranging from 2 to 300 K (see caption of Fig. 5). To evaluate the difference between experiment and theory (the EPM parameters were fitted to  $T=0$  K experimental data) we used the empirical Varshni form,<sup>37</sup>

$$E_g(T) = E_g(T=0) - \frac{\alpha T^2}{T + \beta}, \quad (13)$$

The parameters  $\alpha$  and  $\beta$  for GaSb, InAs, GaAs, and InSb are given in Ref. 5. For the quaternary alloy with In composition  $y$  and As composition  $x$  we estimated the  $\alpha$  and  $\beta$  parameters using a linear interpolation of the binary  $\alpha$  and  $\beta$  values, using an expression of the form as in Eq. (1). We can see in Fig. 5(b) that the  $T=0$  K translated experimental data lie between the dashed line corresponding to the relation for  $E_g$  at  $T=0$  K proposed in Ref. 5 and our calculated values, and there is a difference of the order of about 30 meV at  $y=0.16$  among the band-gap values measured by different groups. Our calculated values are always slightly larger than the experimental data for  $y>0.1$  and the deviation between experiment and theory seems to increase with increasing In (and As) content. Unfortunately, in the energy range  $0.30 < y < 0.70$ , where the differences between the predictions of the atomistic calculations and of the interpolative schemes are larger, the quaternary alloy presents a miscibility gap.<sup>28</sup> Until recently only two lattice-matched regions with indium content  $0 < y < 0.28$  and  $y > 0.70$  were successfully grown and only for these compositions measurements of the band gaps have been performed. Reference 28 reports the measurement of a minimum gap  $E_g=0.34$  eV at  $T=77$  K and  $E_g=0.26$  eV at  $T=300$  K, smaller than the gap of InAs, for the quaternary alloy with  $y>0.70$ . Our calculations predict gaps from 0.27 to 0.35 eV in the range  $x>0.75$  in reasonable agreement with the experimental values.

Experimental values of  $E_g$  of  $\text{Ga}_{1-y}\text{In}_y\text{As}_x\text{Sb}_{1-x}/\text{InAs}$  as a function of composition ( $x, y$ ) are scarce. Moiseev *et al.*<sup>36</sup> measured the photoluminescence (PL) spectra for  $\text{Ga}_{1-y}\text{In}_y\text{As}_x\text{Sb}_{1-x}/\text{InAs}$  in the GaSb-rich range, while Gong *et al.*<sup>38</sup> also did PL measurements in the InAs-rich range. We report the  $T=0$ -K translated band gaps in Fig. 7(b) for comparison with our theoretical predictions. The experimental band gaps are about 50–60 meV smaller than the calculated values on the GaSb-rich side, while they are slightly below the experimental data on the InAs-rich side. However, more experimental data are necessary to derive a clear conclusion about the comparison of experiment and theory for  $\text{Ga}_{1-y}\text{In}_y\text{As}_x\text{Sb}_{1-x}/\text{InAs}$  alloys.

## B. Taking short-range order into account

GaInAsSb alloys are never truly random. To evaluate the deviation from randomness in real alloys grown at a temperature  $T$ , we have applied a finite-temperature Monte Carlo (MC) simulation using “spin-flip+atomic relaxation” steps<sup>39</sup> to the 512 atom unit cell to minimize the energy functional of Eq. (3). We consider  $\text{Ga}_{1-y}\text{In}_y\text{As}_x\text{Sb}_{1-x}/\text{GaSb}$  at  $x=0.1328$  and  $y=0.1875$ , that is at a composition for which different experimental data for the band-gap exist. We obtain  $\xi(x, y, T)=0.024$  at  $T=600$  °C [which is of the order of alloy growth temperature by liquid-phase epitaxy (LPE) and molecular-beam epitaxy (MBE)], while, for example, at  $T$  close to 0 K the SRO parameter is  $\xi(x, y, T)=0.071$ . The results show that for GaInAsSb,  $\xi > 0$ , i.e., the GaSb+InAs configuration is preferred. A SRO with parameter  $\xi=0.024$  leads to a 15–20 meV of  $E_g$  reduction with respect to the

case of  $\xi \approx 0$ . This behavior could explain why the measured values are always below our calculated values in Fig. 5.

On the other hand, the presence of a miscibility gap in the quaternary alloy would lead to some clustering even in molecular-beam epitaxy growth, with spatial fluctuations of the gap. Optical measurements (both absorption and emission) would be dominated by the lower gap, hence one would expect optically obtained gaps to be lower than those in a perfectly random alloy. This could be yet another reason for the observed underestimation of the gap.

## VII. SUMMARY

We applied the atomistic empirical pseudopotential theory, using recently developed potentials for Ga, In, As, and Sb atoms, together with the atomistic elasticity theory, via a valence force field approach, to calculate the evolution of the valence- and conduction-band edges of the quaternary  $\text{Ga}_{1-y}\text{In}_y\text{As}_x\text{Sb}_{1-x}$  alloys grown lattice matched to GaSb and InAs. Our results have been compared with the results of the standard interpolative schemes widely employed by the device engineers to design devices and predict performances. We have found that the use of Vegard’s law, extended to quaternary systems predicts an almost linear behavior for the lattice-matching condition  $x=f_{\text{Vegard}}(y)$ , which links the As fraction  $x$  in the alloy to the In fraction  $y$ , so as to maintain the quaternary  $\text{Ga}_{1-y}\text{In}_y\text{As}_x\text{Sb}_{1-x}$  very closely lattice-matched to its substrate (GaSb or InAs). Our atomistic calculations, however, produce a  $x=f_{\text{VFF}}(y)$  relation with a larger bowing than  $x=f_{\text{Vegard}}(y)$ . However, when used in the EPM band structure calculations, the two lattice-matching functions  $x=f_{\text{Vegard}}(y)$  and  $x=f_{\text{VFF}}(y)$  produce very similar band-edge energies.

A large deviation between our calculated band edges and the predictions of the interpolative schemes has been found. In particular, we have found a negative bowing of the quaternary alloy conduction-band edge  $E_c(y)$  with respect to the end-points GaSb and  $\text{InAs}_{0.89}\text{Sb}_{0.11}$  (for growth on GaSb) and with respect to InAs and  $\text{GaAs}_{0.08}\text{Sb}_{0.92}$  (for growth on InAs), in contrast with the interpolative models which predict large positive bowing of  $E_c$ . We investigated this issue finding a strong effect on the negative bowing of the band-edge energies of the highly strained In–Sb and Ga–As bonds within the alloy, whose presence is ignored or underestimated by the interpolative schemes.

Finally, we have determined at which In composition  $y$  [and As composition  $x$  via  $x=f_{\text{VFF}}(y)$ ] the quaternary alloys change their lineups relative to their substrate from a staggered (type II) to a broken-gap (type III) lineup, and we have determined if a minimum gap (e.g., smaller than the InAs band gap) can be reached using the quaternary  $\text{Ga}_{1-y}\text{In}_y\text{As}_x\text{Sb}_{1-x}$  alloys. We found a positive answer to this question for the quaternary  $\text{Ga}_{1-y}\text{In}_y\text{As}_x\text{Sb}_{1-x}$  alloy grown on an InAs substrate at As and In compositions around  $x=0.85$  and  $y=0.87$ , respectively.

We discussed the implications of our findings for device design and compared our results with the few available experimental data in literature.

## ACKNOWLEDGMENTS

One of the authors (R.M.) acknowledges the European Office of Aerospace Research and Development (EOARD) under Contract No. FA8655-03-1-3017. Another author (A.Z.) acknowledges the US DOE-SC-BES-DMS under Contract No. DEAC36-98-G010337.

- <sup>1</sup>J. R. Meyer *et al.*, IEE Proc.: Optoelectron. **145**, 275 (1998).
- <sup>2</sup>S.-H. Wei and A. Zunger, Appl. Phys. Lett. **72**, 2011 (1998).
- <sup>3</sup>R. Magri and A. Zunger, Phys. Rev. B **65**, 165302 (2002); **64**, 081305(R) (2001); **68**, 155329 (2003).
- <sup>4</sup>C. W. Leitz, M. T. Currie, M. L. Lee, Z.-Y. Cheng, D. A. Antoniadis, and E. A. Fitzgerald, Appl. Phys. Lett. **79**, 4246 (2001).
- <sup>5</sup>I. Vurgaftman, J. Meyer, and L. R. Ram-Mohan, J. Appl. Phys. **89**, 5815 (2001).
- <sup>6</sup>L. Vegard, Z. Phys. **5**, 17 (1921).
- <sup>7</sup>C. Pryor, J. Kim, L. W. Wang, A. J. Williamson, and A. Zunger, J. Appl. Phys. **83**, 2548 (1996).
- <sup>8</sup>G. W. Turner and H. K. Choi, in *Antimonide-Related Strained-Layer Heterostructures*, edited by M. O. Manasreh (Gordon and Breach, New York, 1997), p. 369.
- <sup>9</sup>K. Kim and A. Zunger, Phys. Rev. Lett. **86**, 2609 (2001).
- <sup>10</sup>W. A. Harrison, *Electronic Structure and the Properties of Solids* (Dover, New York, 1989), p. 176.
- <sup>11</sup>P. Keating, Phys. Rev. **145**, 637 (1966).
- <sup>12</sup>J. L. Martins and A. Zunger, Phys. Rev. B **30**, 6217 (1986).
- <sup>13</sup>R. Magri, L. L. Wang, A. Zunger, I. Vurgaftman, and J. R. Meyer, Phys. Rev. B **61**, 10235 (2000).
- <sup>14</sup>*Semiconductors: Group IV and III-V Compounds*, Landolt-Börnstein, New Series, Group III, Vol. 17, edited by O. Madelung (Springer, Berlin, 1982); *Semiconductors: Intrinsic Properties of Group IV Elements and III-V, II-VI and I-VII Compounds*, Landolt-Börnstein, New Series, Group III, Vol. 22, edited by O. Madelung (Springer, Berlin, 1987).
- <sup>15</sup>S.-H. Wei and A. Zunger, Appl. Phys. Lett. **72**, 2011 (1998).
- <sup>16</sup>S.-H. Wei and A. Zunger, Phys. Rev. B **49**, 14337 (1994).
- <sup>17</sup>A. Zunger and A. J. Freeman, Phys. Rev. B **16**, 2901 (1977).
- <sup>18</sup>R. Magri, S. Froyen, and A. Zunger, Phys. Rev. B **44**, 7947 (1991).
- <sup>19</sup>G. C. Dente and M. L. Tilton, J. Appl. Phys. **86**, 1420 (1999); Phys. Rev. B **66**, 165307 (2002).
- <sup>20</sup>R. Magri and A. Zunger, Phys. Rev. B **62**, 10364 (2000), and references therein.
- <sup>21</sup>O. Krebs and P. Voisin, Phys. Rev. Lett. **77**, 1829 (1996).
- <sup>22</sup>Y. A. Bychkov and E. I. Rashba, J. Phys. C **17**, 6039 (1984).
- <sup>23</sup>M. J. Yang, W. J. Moore, B. R. Bennett, and B. V. Shanabrook, Electron. Lett. **34**, 270 (1998); M. J. Yang *et al.*, J. Appl. Phys. **86**, 1796 (1999).
- <sup>24</sup>C. L. Canedy, W. W. Bewley, C. S. Kim, M. Kim, I. Vurgaftman, and J. R. Meyer, J. Appl. Phys. **94**, 1347 (2003).
- <sup>25</sup>D. Gershoni, C. H. Henry, and G. A. Baraff, IEEE J. Quantum Electron. **29**, 2433 (1993).
- <sup>26</sup>W. H. Lau and M. E. Flatte, Appl. Phys. Lett. **80**, 1683 (2002).
- <sup>27</sup>F. Szmulowicz, H. Haugan, and G. J. Brown, Phys. Rev. B **69**, 155321 (2004).
- <sup>28</sup>M. P. Mikhailova and A. N. Titkov, Semicond. Sci. Technol. **9**, 1279 (1994).
- <sup>29</sup>F. Karouta, H. Mani, F. Jia Hua, and A. Jouillie, Rev. Phys. Appl. **22**, 1459 (1987).
- <sup>30</sup>J. C. DeWinter, M. A. Pollack, A. K. Srivastava, and J. L. Zyskind, J. Electron. Mater. **14**, 729 (1985).
- <sup>31</sup>M. J. Cherng, G. B. Stringfellow, D. W. Kisker, A. K. Srivastava, and J. L. Zyskind, Appl. Phys. Lett. **48**, 419 (1986).
- <sup>32</sup>M. Astles, H. Hill, A. J. Williams, P. J. Wright, and M. L. Young, J. Electron. Mater. **15**, 41 (1986).
- <sup>33</sup>J. Shin, T. C. Hsu, Y. Hsu, and G. B. Stringfellow, J. Cryst. Growth **179**, 1 (1997).
- <sup>34</sup>H. Kroemer (unpublished).
- <sup>35</sup>T. I. Voronina, B. E. Zhurtanov, T. S. Lagunova, M. P. Mikhailova, K. D. Moiseev, A. E. Rozov, and Yu. P. Yakovlev, Semiconductors **35**, 331 (2001).
- <sup>36</sup>K. D. Moiseev, A. A. Toropov, Ya. V. Terent'ev, M. P. Mikhailova, and Yu. P. Yakovlev, Semiconductors **34**, 1432 (2000).
- <sup>37</sup>Y. P. Varshni, Physica (Amsterdam) **34**, 149 (1967).
- <sup>38</sup>X. Gong, H. Kan, T. Yamaguchi, I. Suzuki, M. Aoyama, M. Kumagawa, N. L. Rowell, A. Wang, and R. Rinfret, Jpn. J. Appl. Phys., Part 1 **33**, 1740 (1994).
- <sup>39</sup>A. Silverman, A. Zunger, R. Kalish, and J. Adler, Phys. Rev. B **51**, 10795 (1995).